

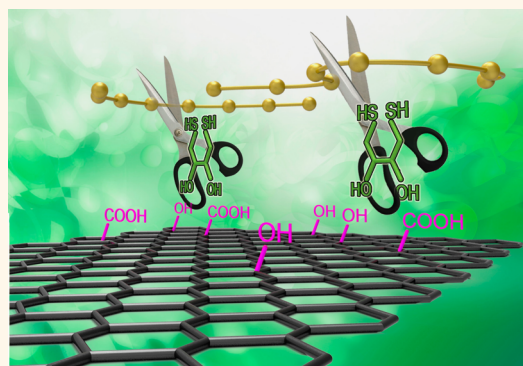
Polysulfide-Scission Reagents for the Suppression of the Shuttle Effect in Lithium–Sulfur Batteries

Wuxing Hua, Zhi Yang,*^{1b} Huagui Nie, Zhongyu Li, Jizhang Yang, Zeqing Guo, Chunping Ruan, Xi'an Chen, and Shaoming Huang*

Nanomaterials & Chemistry Key Laboratory, Wenzhou University, Wenzhou 325027, China

S Supporting Information

ABSTRACT: Lithium–sulfur batteries have become an appealing candidate for next-generation energy-storage technologies because of their low cost and high energy density. However, one of their major practical problems is the high solubility of long-chain lithium polysulfides and their infamous shuttle effect, which causes low Coulombic efficiency and sulfur loss. Here, we introduced a concept involving the dithiothreitol (DTT) assisted scission of polysulfides into lithium–sulfur system. Our designed porous carbon nanotube/S cathode coupling with a lightweight graphene/DTT interlayer (PCNTs-S@Gra/DTT) exhibited ultrahigh cycle-ability even at 5 C over 1100 cycles, with a capacity degradation rate of 0.036% per cycle. Additionally, the PCNTs-S@Gra/DTT electrode with a 3.51 mg cm⁻² sulfur mass loading delivered a high initial areal capacity of 5.29 mAh cm⁻² (1509 mAh g⁻¹) at current density of 0.58 mA cm⁻², and the reversible areal capacity of the cell was maintained at 3.45 mAh cm⁻² (984 mAh g⁻¹) over 200 cycles at a higher current density of 1.17 mA cm⁻². Employing this molecule scission principle offers a promising avenue to achieve high-performance lithium–sulfur batteries.



KEYWORDS: lithium–sulfur batteries, porous carbon nanotube, polysulfide-scission, interlayer, dithiothreitol

A wealth of interdependent research into high-energy-density rechargeable batteries with long-lasting cycle performance is being explored to promote the practical applications of electric vehicles and large-scale smart grids. Beyond the limitations of the Li-ion battery, lithium–sulfur (Li–S) batteries show promising potential as next-generation energy-storage technologies because of their low cost, eco-friendliness, high theoretical capacity and energy density.^{1–4} Despite these considerable advantages, practical applications of rechargeable Li–S batteries remain a challenge—hindered by several issues, such as poor sulfur conductivity, high volume expansion during cycling, and the dissolution of intermediate lithium polysulfide products (LiPSs, Li₂S_n, 4 ≤ n ≤ 8), leading to notorious shuttle effects,^{5–8} thereafter resulting in high self-discharge, low Coulombic efficiency, and active material loss.

Recent efforts, such as impregnating sulfur into high conductive and adsorptive hosts (e.g., graphene,⁹ hollow porous spheres^{10,11}) and coupling with specific inorganic anchoring materials (e.g., Ti₄O₇^{6,12} and MnO₂^{13,14}), have been devoted to addressing these obstacles, especially the shuttle effect. The introduction of a carbon-based interlayer between the cathode and separator is a recently useful technique developed for

intercepting the migrating PSs followed by subsequent reuse of the trapped active materials.^{15–18} Our group further designed a lightweight, chemically selective TiO₂/graphene interlayer as a Li–S battery component yielding excellent cycling stability at a relatively high rate (3 C).¹⁹ Regardless of recently significant successes when adopting such methods, namely preventing LiPSs diffusion, it was noted that unavoidable soluble LiPSs arise and accumulate in the electrolyte during the transformation from S to Li₂S. Once the phenomenon appears, active sulfur species lose intimate contact sites with the conductive matrix, resulting in an increase of internal resistance.^{20,21} Fast accumulation of LiPSs in the electrolyte coupled with slow conversion reaction kinetics further hinder electron and ion transport in the electrode and electrolyte, resulting in fast capacity decay. In this regard, eliminating or rapidly converting LiPSs residing at the electrolyte requires further investigation by the scientific community to circumvent the flooding of LiPSs. In the past few years, Guo²² *et al.*

Received: December 24, 2016

Accepted: February 1, 2017

Published: February 1, 2017

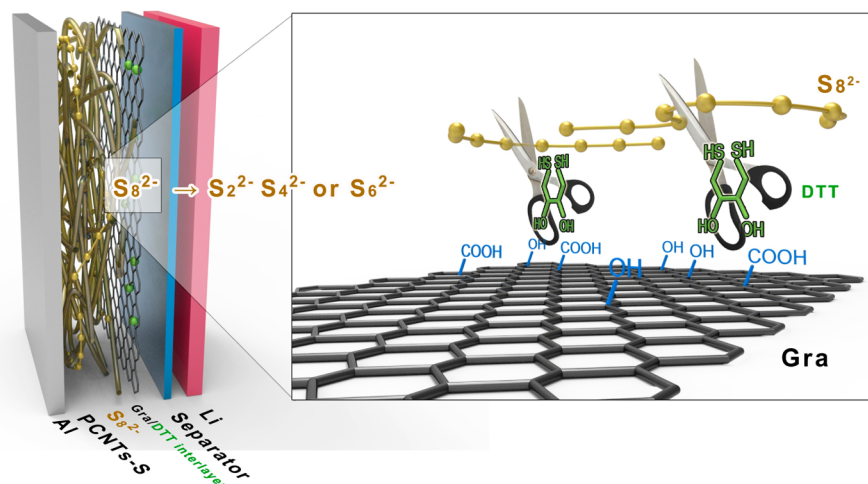


Figure 1. Schematic of electrode configuration for Li–S battery with Gra/DDT interlayer.

employed a microporous carbon to confine small S_{2-4} molecules, avoiding the unfavorable formation of soluble PSs, and thus delivering impressive electrochemical properties. However, the rigorous preparation process to control the narrow micropore size distribution, in addition to the small microporous volume, may be a significant barrier for large-scale practical applications. Recently, Arava²³ *et al.* applied an electrocatalysis principle to a specific Li–S battery configuration to stabilize the LiPSs shuttle process. Observations revealed that Pt/graphene catalysts promote the transformation of long-chain PSs in the subsequent redox process. Very recently, Zhang²⁴ *et al.* confirmed that introducing CoS_2 into the S cathode results in significant enhancement of the redox reactivity of LiPSs, yielding high discharge capacities, in addition to enhancing cycling stability. Introducing various catalysts or functional materials to greatly suppress shuttle effect has become a fashionable strategy in Li–S fields.^{25–27} In this respect, developing neoteric functional molecules, which can achieve rapid conversion of LiPSs at room temperature, is highly desired to further manage the LiPSs shuttle effect.

Biocatalysts or bioinspired catalysts may be an ideal choice to address the aforementioned issue owing to their superior catalytic performance under mild reaction conditions, compared with traditional catalysts.²⁸ Furthermore, it is worth noting that the disulfide ($-S-S-$) bond plays an important role in the structural features of many proteins, allowing protein folding and stability to be maintained.²⁹ The most important aspect involving disulfide bonds is their cleavage, which occurs *via* the reaction to slice the $-S-S-$ bonds. In biochemistry, biological reagents, such as vitamin C (VC), glutathione (G-SH) and dithiothreitol (DTT), are often used to fast slice the disulfide bonds at room temperature.^{30,31}

Inspired by these facts, herein we introduced a concept involving the dithiothreitol assisted scission of LiPSs, and designed a Li–S battery configuration consisting of a porous carbon nanotube/S cathode (PCNTs-S) coupled to a light-weight graphene/dithiothreitol (Gra/DDT) interlayer, where the introduced DTT can rapidly eliminate the accumulation of LiPSs *via* the reaction to slice the $-S-S-$ bonds. By virtue of the special functionality, the Gra/DDT interlayer enables the PCNTs-S cathode to deliver a much higher initial discharge capacity of 1643 mAh g^{-1} at a current rate of 0.2 C and a reversible specific capacity of 880 mAh g^{-1} over 400 cycles was achieved at a current rate of 1 C, corresponding to an ultralow-

capacity degradation rate of 0.029% per cycle. Remarkably, our studies further confirmed that when cycled at 5 C over 1100 cycles, the cathode maintained ultrahigh cycling ability, with a capacity degradation rate of 0.036% per cycle. To the best of our knowledge, such excellent performance at an ultrahigh rate of 5 C in Li–S batteries has rarely been reported. Additionally, the PCNTs-S@Gra/DDT electrode with a 3.51 mg cm^{-2} sulfur mass loading delivered a high initial areal capacity of 5.29 mAh cm^{-2} (1509 mAh g^{-1}) at current density of 0.58 mA cm^{-2} , and the reversible areal capacity of the cell was maintained at 3.45 mAh cm^{-2} (984 mAh g^{-1}) over 200 cycles at a higher current density of 1.17 mA cm^{-2} , which represents a high Capacity retention rate of 78.5%. More importantly, this design idea involving the DTT assisted scission of LiPSs can be further extended to other biological reagents, such as VC and G-SH. Subsequent development of Gra/VC and Gra/G-SH interlayers show that various other PCNTs/S cathodes comprising biological reagents also display significant superior electrochemical performance compared with alternative cathodes.

RESULTS AND DISCUSSION

A schematic illustration of the cell configuration is shown in Figure 1. Different from conventional Li–S batteries, our electrode design introduces a Gra/DDT interlayer inserted between the cathode and separator. Photographs illustrate the cathode fabrication process (Supporting Information Figure S2a, b): a conventional sulfur cathode with a PCNTs host material, as reported in our previous studies,^{19,32} was prepared *via* a facile coating method, subsequently followed by overlaying the Gra/DDT interlayer onto the sulfur cathode; the obtained cathode is named PCNTs-S@Gra/DDT. The diagrammatic drawing in Supporting Information Figure S2c clearly shows the structure of the PCNTs-S@Gra/DDT cathode. The mass of the interlayer was determined by weighing the electrode prior to and after the double-coating, from a cross-sectional area loading of $\sim 0.07 \text{ mg cm}^{-2}$ —lighter than the majority of the reported free-standing interlayers.^{15–19} Standard 2025 coin cells were fabricated using a PCNTs-S@Gra/DDT cathode *vs* a metallic lithium anode and dissolved $LiNO_3$ in an electrolyte. For a more relevant comparison, we also fabricated PCNTs-S, PCNTs-S@Gra, PCNTs-S-DDT@Gra and CNTs-S@Gra/DDT cathodes. In this work, we selected PCNTs samples obtained *via* a high-temperature

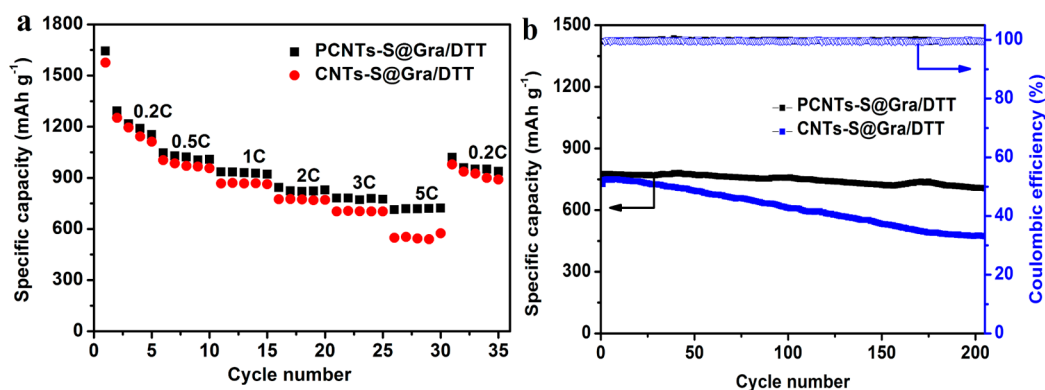


Figure 2. Contrast of electrochemical performance between PCNTs-S@Gra/DTT and CNTs-S@Gra/DTT cathodes. (a) The rate performance of PCNTs-S@Gra/DTT and CNTs-S@Gra/DTT cathodes. (b) Cycling stability of PCNTs-S@Gra/DTT and CNTs-S@Gra/DTT cathodes at 3 C.

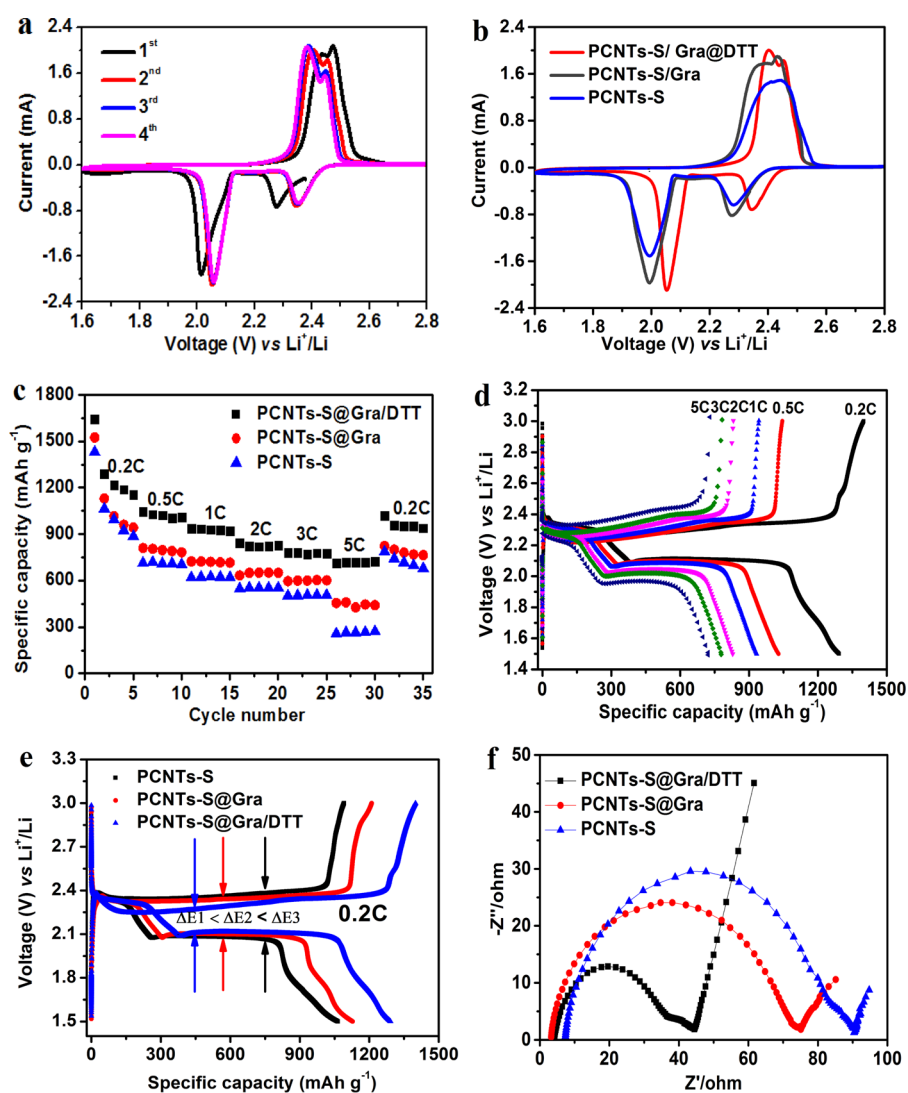


Figure 3. Electrochemical performance of lithium-sulfur batteries. (a) The first four cycles of CV profiles for PCNTs-S@Gra/DTT cathode. (b) The second cycle of CV profiles for PCNTs-S, PCNTs-S@Gra, and PCNTs-S@Gra/DTT cathodes. (c) The rate performance of PCNTs-S@Gra/DTT, PCNTs-S@Gra, and PCNTs-S cathodes, the areal loading amount of sulfur in the rate test is 0.49 mg/cm^2 . (d) Galvanostatic charge-discharge profiles of the PCNTs-S@Gra/DTT cathode at various rates. (e) Galvanostatic charge-discharge profiles of the PCNTs-S@Gra/DTT, PCNTs-S@Gra, and PCNTs-S cathodes at 0.2 C. (f) Electrochemical impedance spectroscopy of the three cathodes.

reaction between the crude CNTs and a nebulized water stream^{19,32} for the subsequent Li-S battery experiments.

Supporting Information Figure S3 shows the pore size distribution and Nitrogen adsorption-desorption isotherms

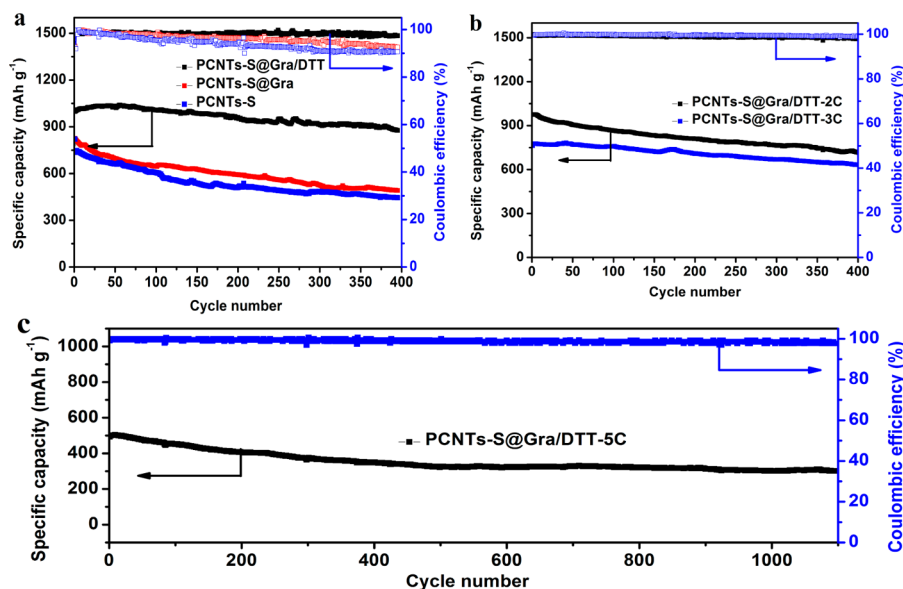


Figure 4. Long cycling performance of lithium-sulfur batteries: (a) Cycling stability of PCNTs-S@Gra/DTT, PCNTs-S@Gra, and PCNTs-S cathodes at 1 C. (b) Cycling performance of PCNTs-S@Gra/DTT cathode at 2 and 3 C. (c) Prolong cyclic stability of PCNTs-S@Gra/DTT cathode at high current of 5 C. The areal loading amount of sulfur is 0.49 mg/cm^2 at 1, 2, 3 and 5 C in the cycling test.

of the as-obtained PCNTs and crude CNTs. The rate performance and cycle stability for PCNTs-S@Gra/DTT and CNTs-S@Gra/DTT are shown in Figure 2, which confirms that the cell with PCNTs-S displays significantly enhanced electrochemical performance compared with the cell produced using crude CNTs-S composites after introducing the Gra/DTT interlayer. Therefore, all host materials herein use PCNTs, if not specifically mentioned.

Cyclic voltammetry (CV) plots of the PCNTs-S@Gra/DTT cathode for the initial four cycles are shown in Figure 3a, recorded at a slow scan rate of 0.1 mV s^{-1} . In the first cathode scan, two characteristic reduction peaks at 2.28 and 2.01 V can be observed, corresponding to the disproportion of long-chain PS (Li_2S_n , $4 \leq n \leq 8$) and formation of Li_2S_2 and Li_2S , respectively. In relation to the forward scan, two distinguishable oxidation peaks are observed at 2.43 and 2.47 V, which are attributed to the conversion of short-chain to long-chain LiPS, and finally to elemental sulfur.^{4,9,16,19,23,32} The large variation in the reduction and oxidation peaks between the first and second cycles is ascribed to the rearrangement of active sulfur from its original positions to more energetically stable sites.^{19,32} Compared with the four nonoverlapping CV plots of the PCNTs-S and PCNTs-S@Gra cathodes (Supporting Information Figure S4), the almost identical CV plots for the PCNTs-S@Gra/DTT cathode in the subsequent two cycles indicate that the PCNTs-S@Gra/DTT cathode possesses higher reversible electrochemical properties.^{33,34} Figure 3b shows the second cycle of the CV plots for the three cathodes. The PCNTs-S@Gra/DTT cathode exhibits the highest collection coefficient (the ratio of the peak areas associated with the formation of Li_2S , at $\sim 2.0 \text{ V}$, to that of the formation of LiPSs, at $\sim 2.4 \text{ V}$) of 2.847, compared with 2.406, and 2.401 for the PCNTs-S@Gra and PCNTs-S cathodes, respectively, evidencing that the Gra/DTT interlayer promotes a fast conversion reaction of LiPS and effectively inhibits the shuttle effect.¹⁹ Additionally, when comparing the CV of the PCNTs-S@Gra and PCNTs-S cathodes, a distinguishable positive shift in the PCNTs-S@Gra/DTT cathode reduction peak can be observed,

which confirms a relatively low potential polarization together with good cell reversibility as a direct result of the Gra/DTT interlayer insertion.³⁵ An interesting point to note is that the starting position of oxidation peak for the PCNTs-S@Gra/DTT cathode is shifted to a higher voltage than those of the PCNTs-S and PCNT-S@Gra cathodes. We speculated that this upshift of the starting position for the oxidation peak may be the root cause in decreasing the PS species in the presence of the DTT molecules possessing polysulfide-scission functionality. Furthermore, from Supporting Information Table S1, the PCNTs-S@Gra/DTT cathode also showed the lowest voltage hysteresis (ΔV) among the three cathodes, suggesting a highly facile electrochemical redox reaction and low resistance.¹⁹

Figure 3c exhibits the rate performance of the three cathodes ranging from 0.2 to 5 C ($1 \text{ C} = 1675 \text{ mA g}^{-1}$) and the charge-discharge curves of the PCNTs-S@Gra/DTT cathode at various current rates (0.2–5 C) are illustrated in Figure 3d. Compared with the PCNTs-S and PCNTs-S@Gra batteries, the PCNTs-S@Gra/DTT battery delivers a much higher initial capacity of 1643 mAh g^{-1} at the rate of 0.2 C, followed by a subsequent slow decrease to 1046, 935, and 843 mAh g^{-1} at rates of 0.5, 1, and 2 C, respectively. Even at higher rates of 3 and 5 C, a reversible capacity of 781 and 712 mAh g^{-1} can still be achieved. When abruptly switching the rate from 5 C back to the initial starting rate of 0.2 C, the original capacity was largely recovered, indicating the excellent reversible capacity of the PCNTs-S@Gra/DTT battery at various rates.

In Figure 3e, the galvanostatic charge-discharge profiles at 0.2 C for the three cathodes also showed that the PCNTs-S@Gra/DTT cathode had the lowest voltage hysteresis (ΔE), in agreement with the polarized voltage (ΔV) from the CV plots (Supporting Information Table S1). These results suggested that introducing DTT into the Li-S system can sufficiently promote the reduction of the intermediate LiPSs to $\text{Li}_2\text{S}_2/\text{Li}_2\text{S}$, in addition to increasing the utilization of sulfur materials.^{19,36} Electrochemical impedance spectroscopy (EIS) data (Figure 3f) and the corresponding electrical equivalent circuit diagram (Figure S5a, b) showed that the PCNTs-S@Gra/DTT cathode

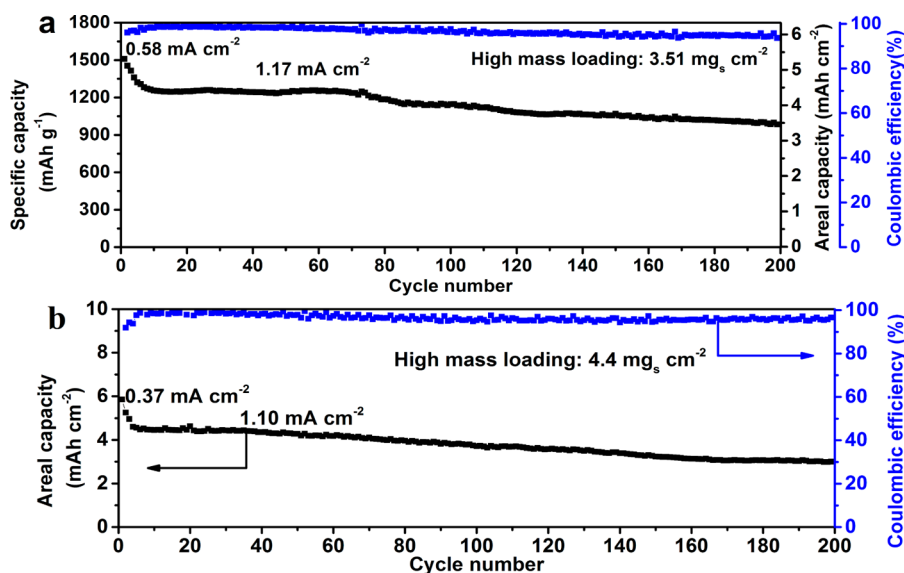


Figure 5. (a, b) The cycling performance of PCNTs-S@Gra/DTT with different sulfur mass loading.

has the lowest charge-transfer resistance (R_{ct}) value, indicating a low resistance caused by the entrapment of the dissolved PSs and both good electrolyte infiltration and charge transport. Furthermore, it is also noteworthy that the Nyquist EIS of the PCNTs-S@Gra/DTT cathode displays two semicircles, presenting different properties to the PCNTs-S@Gra cathode. Combined with the fitted equivalent circuit diagram in Figure S5a, it is speculated that the first semicircle at high frequency is represented by $R_1//CPE_1$, which is attributed to the charge transfer resistance and a pore double layer capacity in the surface corresponding the PCNTs-S layer.²¹ The second semicircle in the midfrequency region may be caused by the redox reaction between the DTT and LiPS species at the introduced interlayer surface.

Cycling stability is an important indicator to evaluate the property of Li-S batteries. Compared with the PCNTs-S and PCNTs-S@Gra batteries, the cathode with Gra/DTT as the interlayer exhibited a significantly higher initial discharge capacity of 997 mAh g^{-1} , reducing to 880 mAh g^{-1} after 400 cycles at 1 C (Figure 4a), corresponding to a low-capacity decay rate of 0.029% per cycle. Additionally, the PCNTs-S@Gra/DTT cathode had the highest Coulombic efficiency among the three cathodes over 400 cycles, proving that the Gra/DTT interlayer can effectively suppress the notorious shuttle effect and improve the cycling stability.^{12,37} Furthermore, the EIS spectra in Supporting Information Figure S5c, d, e showed that the PCNTs-S@Gra/DTT exhibited the lowest R_{ct} among the three cathodes before and after cycling, indicating that the dissolution of LiPSs was effectively suppressed.^{36,38}

The long-term cycling stability of the PCNTs-S@Gra/DTT cathode was also tested at high current rates. At a current rate of 2 C, an initial capacity of 975 mAh g^{-1} was achieved. This capacity decreased to 723 mAh g^{-1} after 400 cycles, which represents a capacity decay rate of 0.064% per cycle. When increasing the current rate to 3 C, an improved cycle stability was achieved, and the capacity decreased from 762 to 635 mAh g^{-1} after 400 cycles, which represents a lower decay rate of 0.041% per cycle. Additionally, the average Coulombic efficiency of the PCNTs-S@Gra/DTT cathode improved from 98.9% at 2 C to 99.5% at 3 C (Figure 4b), agreeing

with a previous report⁹ that the shuttling effect can effectively be prevented as a function of increasing current rate because of a significantly faster charge-discharge process. Typical charge-discharge profiles in the second, 100th, 200th and 400th cycles show a slight increase in ΔV after 400 cycles at 2 and 3 C (Supporting Information Figure S6), suggesting an improved stability of the cathode and less PSs dissolution into the electrolyte. More importantly, further increasing the current density to 5 C resulted in an available useable capacity of 301 mAh g^{-1} being maintained after 1100 cycles, corresponding to a very small capacity decay of 0.036% per cycle and a high-capacity retention rate of 60% (Figure 4c). The PCNTs-S@Gra/DTT cathode shows a promising potential for electric vehicles and large-scale electrochemical energy-storage systems. To our best knowledge, such a high-capacity retention rate at 5 C has rarely been reported.

To further evaluate the PCNTs-S@Gra/DTT cathode for practical high-power applications, three half-cells consisting of 1.47 mg of S were assembled in series. With an open-circuit-potential of 6.83 V, the device could efficiently drive 60 green indicators of LED modules (nominal voltage is 12 V, nominal power is 3 W) after only 60 s of charging at 1 C (Supporting Information Figure S7), meaning that the instantaneous current and power of the device are as high as 298.8 A g^{-1} and 2040.8 W g^{-1} , respectively, superior to a recent report.³⁹ These results revealed the outstanding high-power performance of the PCNTs-S@Gra/DTT cathode, which is among state-of-the-art energy-storage devices.

Targeting practical applications of Li-S batteries, a sulfur loading area of $>3 \text{ mg cm}^{-2}$ was applied to satisfy the requirements of HEV and EV batteries.⁴⁰ A PCNTs-S@Gra/DTT cathode with 3.51 mg cm^{-2} sulfur areal loading was fabricated as a function of increasing electrode thickness and sulfur content (76 wt %, Supporting Information Figure S8). The PCNTs-S@Gra/DTT electrode (Figure 5a) with 3.51 mg cm^{-2} sulfur mass loading delivered a high initial areal capacity of 5.29 mAh cm^{-2} (1509 mAh g^{-1}) at current density of 0.58 mA cm^{-2} , and the reversible areal capacity of the cell was maintained at 3.45 mAh cm^{-2} (984 mAh g^{-1}) over 200 cycles at a higher current density of 1.17 mA cm^{-2} , which represents a high Capacity retention rate of 78.5%. Additionally, another

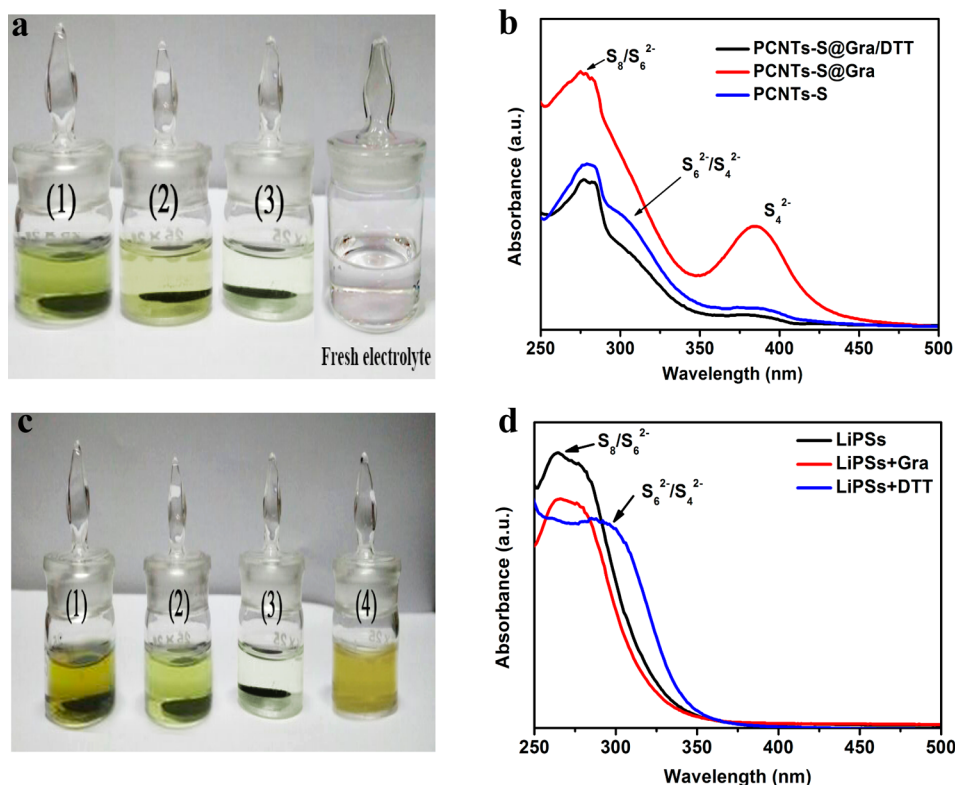


Figure 6. Polysulfide permeation measurements. (a) Typical colors of electrolyte for the PCNTs-S (1), PCNTs-S@Gra (2) and PCNTs-S@Gra/DTT (3) cathodes after 50 cycles in sealed vials. (b) UV-vis absorption spectra of the solution obtained by soaking the cycled PCNTs-S, PCNTs-S@Gra, and PCNTs-S@Gra/DTT cathodes in a mixture of DOL/DME. (c) Visualized color change after PCNTs-S, PCNTs-S@Gra, PCNTs-S@Gra/DTT cathodes immersing in (1), (2), (3) solution for 6 h, respectively, (4) as reference. (d) UV-vis absorption spectra of the solution after soaking fresh PCNTs-S, PCNTs-S@Gra, and PCNTs-S@Gra/DTT cathodes.

PCNTs-S@Gra/DTT cathode with 4.4 mg cm^{-2} sulfur areal loading also exhibited a high areal capacity of 5.85 mAh cm^{-2} at a current density of 0.37 mA cm^{-2} and maintained a high areal capacity of 3.0 mAh cm^{-2} at a higher current density of 1.10 mA cm^{-2} after 200 cycles (Figure 5b). Considering such a high sulfur areal loading in the related electrode, the cyclic performance of the PCNTs-S@Gra/DTT cathode is comparable with recent reported work (Supporting Information Table S2).

To investigate the enhancement mechanism involving DTT for improving the performance of Li-S batteries, we disassembled the cells containing three various cathodes (PCNTs-S, PCNTs-S@Gra and PCNTs-S@Gra/DTT) in the discharged state after 50 cycles at 2 C inside a glovebox. Thereafter, the cathodes were soaked in a mixture of 1,3-dioxolane/1,2-dimethoxyethane (DOL/DME, 1:1 vol:vol) solution for 3 h. As shown in Figure 6a, after soaking the PCNTs-S@Gra/DTT cathode, the color of the solution remains transparent and colorless, suggesting only a negligible amount of soluble LiPSs in the cell with DTT. Conversely, the solutions relating to the PCNTs-S and PCNTs-S/Gra cathodes show a distinct color change from colorless to golden during the soaking, which is direct evidence of soluble LiPSs accumulation. The aforementioned observations strongly confirm that introducing DTT can eliminate the accumulation of LiPSs in the Li-S system. UV-vis absorption spectra measurements were also performed to further understand the result. As shown in Figure 6b, a sharp peak is discernible at 280 nm attributed to S_8 and S_6^{2-} species, and a shoulder peak at 310 nm attributed to S_6^{2-} or S_4^{2-} species for the three solutions,

while a noticeable absorption peak at 385 nm attributed to the S_4^{2-} species is only present corresponding to the solution from the PCNTs-S@Gra cathode.^{19,41,42} Combined with the battery performance for the three electrodes, the UV-vis results further suggest that the graphene interlayer in the absence of DTT can intercept the migrating LiPSs and reuse the trapped active materials in the cathode; however, the mechanical barrier is not available to eliminate the accumulation of LiPSs. The absence of the peak at 385 nm after introducing DTT seems to suggest that DTT can slice the S_4^{2-} species to form solid Li_2S or Li_2S_2 at room temperature.

To further reveal the reaction mechanism between LiPSs and the Gra/DTT interlayer, we prepared a LiPS solution using a short circuit between the PCNTs-S cathode and Li anode in an electrolyte (Supporting Information Figure S9) and the as-obtained LiPS solution is shown in Supporting Information Figure S10a. The three fresh electrodes (PCNTs-S, PCNTs-S@Gra, PCNTs-S@Gra/DTT) were thereafter soaked in the LiPS solution for 6 h, respectively, and solvent (4) was used as a reference. After soaking the PCNTs-S@Gra/DTT cathode, the color of the solvent phase underwent a fast change from golden to colorless, while the two solvents corresponding to the PCNTs-S and PCNTs-S@Gra cathodes only slightly decolorized even after resting for 6 h (Figure 6c). To obtain further insight into the color change, the two solvents in the presence of fresh PCNTs-S@Gra/DTT and PCNTs-S@Gra cathodes were further treated *via* stirring, centrifugation and filtration. From Supporting Information Figure S11, it can be observed that the color of the solvent phase for PCNTs-S@Gra/DTT remained unchanged, while the solvent for PCNTs-S@Gra almost

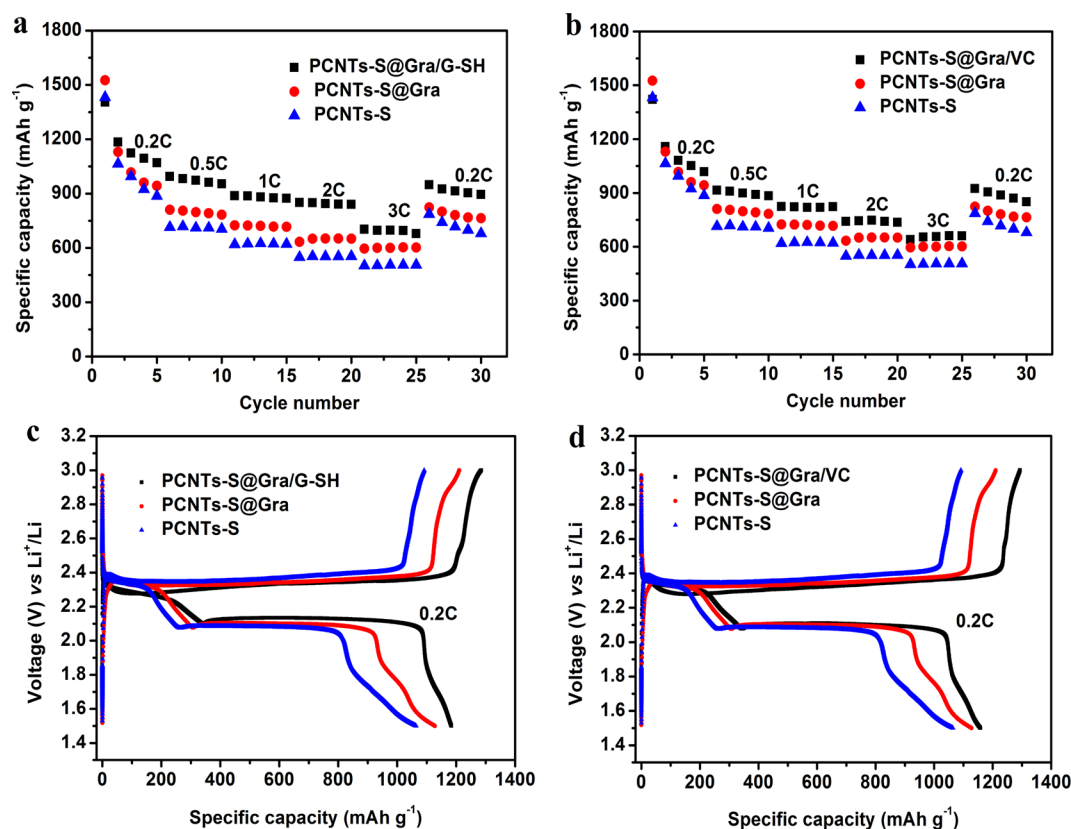
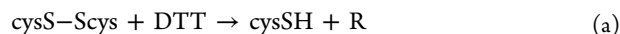
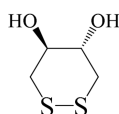


Figure 7. Electrochemical performance of related lithium-sulfur batteries: (a, b) the rate performance of related electrodes; (c, d) galvanostatic charge-discharge profiles of related electrodes at 0.2 C.

recovered to the previous golden color. The sharp contrast confirmed that the conversion reaction of PS on the introduced Gra/DTT interlayer surface results from a chemical change. The UV-vis absorption spectra (Figure 6d) shows that the sharp peak at 280 nm attributed to S_8 and S_6^{2-} species converts to a shoulder peak at 310 nm attributed to S_6^{2-} and S_4^{2-} species after adding DTT into the as-obtained LiPS solution, while no change involving the peak location was discovered after only adding graphene sheets. This result evidence direct proof that DTT can slice the generated LiPSs to short-chain sulfides during cycling of Li-S battery. According to previous reports in biochemistry,^{29–31} DTT is often used to prevent proteins from polymerization by slicing the $-S-S-$ bond, as described by eq a. Herein, we speculate that the introduced DTT in the Li-S battery system maybe also undergo a similar biochemical reaction, as described by eqs b, c and d, thus accelerating the LiPS conversion and avoiding their accumulation in the electrolyte.



R represents:



Considering the scission of LiPSs may affect the distribution of active materials, we further characterized the disassembled PCNTs-S@Gra, and PCNTs-S@Gra/DTT cathodes by SEM. The SEM micrograph of the PCNTs-S@Gra/DTT cathode showed that the distribution of the discharge products was almost homogeneous; little cracks or dendrites were found on the surface of the cathode after cycling at 2 C (Supporting Information Figure S12a). Conversely, the PCNTs-S@Gra cathode appeared porous with agglomerated discharge products and exposed filaments growing out from the granular lithium particles (Supporting Information Figure S12b). The sharp contrast suggested that the Gra/DTT interlayer can help maintain cathode structural integrity, ensuring sufficient paths for electron/ Li^+ -ion transport and channels for electrolyte immersion to undergo electrochemical reactions. On the basis of the aforementioned optical photos, UV-vis absorption measurements, and SEM observations, it is further confirmed that DTT can rapidly eliminate the accumulation of LiPSs *via* $-S-S-$ bond cleavage at room temperature, essentially circumventing the notorious problem relating to the shuttle effect of soluble PSs, ensuring the long-term stable operation of Li-S batteries even at ultrahigh rates. Additionally, in order to further probe into the stability of DTT in the graphene/DTT interlayer, we studied the PCNTs@Gra/DTT cathode in the absence of sulfur loading. In Supporting Information Figure S13a, the cathode exhibited a reversible capacity of 100 mAh g^{-1} (based on DTT weight) at 2 C even after 1000 cycles at the same working conditions. Combining with the high reversible electrochemical property as shown in Figure 3a as well as the observations of the long cycling performance for the PCNTs-S@Gra/DTT cathode (Figure 4), it is believed that DTT as an

electrode material can exist during the long-term operation of Li–S batteries. This may also be an important precondition and strong guarantee to achieve excellent cycling stability in Li–S batteries.

To further probe into the general applicability of biological molecular in Li–S batteries, other biological polysulfide-scission reagents, such as VC and G-SH, were selected as interlayer materials; the relevant constitutional formulas of VC and G-SH are shown in Supporting Information Figure S14. The as-obtained PCNTs-S@Gra/G-SH and PCNTs-S@Gra/VC batteries also exhibited a positive rate performance as shown in Figure 7. Taking the PCNTs-S@Gra/G-SH battery as an exemplary case, the specific capacities are approximately 1404, 993, 888, and 850 mAh g⁻¹ at 0.2, 0.5, 1, and 2 C, superior to PCNTs-S@Gra and PCNTs-S batteries. Abruptly changing the current density back to 0.2 C results in the specific capacity returning to 948 mAh g⁻¹ (Figure 7a), indicating a good stability and reliability of the Gra/G-SH interlayer—preventing PSs shuttle at various current rates. Furthermore, the galvanostatic charge–discharge profiles at 0.2 C for the three cathodes also confirm that the PCNTs-S@Gra/G-SH cathode has the lowest voltage hysteresis (ΔE) (Figure 7c). From Figure 7b and Figure 7d, it can be observed that the Gra/VC interlayer also exhibits the same improved effect as the Gra/G-SH interlayer. These results further evidence the promising route that introducing biological polysulfide-scission reagents can suppress the shuttle effect and improve the electrochemical properties of Li–S batteries.

CONCLUSIONS

In summary, our designed PCNTs-S@Gra/DTT cathode configuration showed significantly enhanced improvements in capacity retention and long-term cycle stability in Li–S batteries. The PCNTs-S cathode coated with a Gra/DTT interlayer delivered a reversible specific capacity of ~880, 723, and 635 mAh g⁻¹ over 400 cycles at 1, 2, and 3 C with high-capacity retention of 88.3%, 74.1%, and 83.3%, respectively. Impressively, the electrode displayed a reversible capacity of 301 mAh g⁻¹ over 1100 cycles with an ultralow-capacity degradation rate of 0.036% per cycle at 5 C. Furthermore, the PCNTs-S@Gra/DTT electrode (3.51 mg cm⁻² sulfur areal loading) delivered a high reversible areal capacity of 3.45 mAh cm⁻² (984 mAh g⁻¹) at a higher current density of 1.17 mA cm⁻² over 200 cycles. Employing this molecule scission principle derived from the introduction of biological reagents, to improve battery properties offers a promising avenue to achieve high-energy-density and long-life cycle Li–S batteries.

EXPERIMENTAL SECTION

Synthesis of Porous CNTs. The porous CNTs were prepared using a water stream etching method as reported in the previous reports.^{19,32,36} Briefly, the water was first nebulized to create a mist of droplets. The droplets formed were then passed into a quartz tube of raw commercial CNTs using an Ar-carrying gas when the desired temperature of 850 °C is reached. After the water etching, the water steams were turned off, and the furnace was cooled to room temperature under argon flow.

Synthesis of PCNTs-S Cathodes. The PCNTs-S composites were prepared following a melt-diffusion strategy. In a typical procedure, the PCNTs and sulfur (high purity sulfur, 99.99% metal basis, Aladdin) were mixed according to the designment of target composite. Then the powder were ground and heated in an oven at 160 °C for 12 h. From Supporting Information Figure S1a–c, it is found that no bulk sulfur particles were formed, and the sulfur was

uniformly distributed in the PCNTs. The sulfur contents in this work were determined to be 63 w %. The cathode for PCNTs-S Cathodes were prepared by mixing 83 wt % PCNT-S composite materials, 12 wt % conductive agent and 5 wt % polyvinylidenedifluoride (PVDF) in NMP to form slurry. After stirring for 1 h, the slurry was pasted onto a aluminum foil and dried at 55 °C overnight.

Synthesis of PCNTs-S@Gra/DTT Cathodes. The graphene and DTT powder were ultrasonically dispersed in NMP to form the graphene/DTT composite slurry. The slurry was then pasted onto the PCNTs-S cathode following procedure shown in Supporting Information Figure S2 to produce PCNTs-S@Gra/DTT cathodes. Considering the thickness of interlayer is an important factor to determine the performance of Li–S battery, in our experiments, the control experiments involved the thickness were also carried out by adjust the slurry's viscosity and the scale of the spreader. To obtain the relatively exact weight data for these pieces, we used two methods as reported in our previous report:¹⁹ (1) In our experiments, to ensure that all components are mixed homogeneously, the slurries of cathode and interlayer were adequately stirred. A similar rectangle PCNTs-S cathode piece was obtained by a spreader, and the Gra/DTT interlayer was subsequently coated on the surface of the cathode piece to obtain the PCNTs-S@Gra/DTT cathode. To prove the homogeneity of these cathode pieces, some small pieces in some different areas for the cathode piece were selected and tailored. The weights (W) and areas (S) of these small pieces were also measured. We found that the values of the areal density ($D = W/S$) of these small pieces from the same sample are quite close if the previous slurry of the cathode was adequately stirred. Therefore, the weight of the cathode can be obtained by the equation ($W = D \times S$), and the weight of the interlayer was determined by obtaining the weight of the electrode before and after the coating process. (2) After ensuring that all previous slurries of cathode and interlayer were adequately stirred, we weighed six same cathodes (W_1) once, and counted their average weight ($W = W_1/6$). We found that the measuring values obtained from the two methods are almost equal.

Synthesis of PCNTs@Gra/DTT Cathode. The cathode was prepared using PCNTs instead of PCNTs-S *via* the same procedure as synthesis of PCNTs-S@Gra/DTT cathode.

Electrochemical Characterization. Electrochemical experiments were performed *via* CR2025 coin-type test cells assembled in an argon-filled glovebox with lithium metal as the counter and reference electrodes at room temperature. Celgard 2400 membrane was used as the separator to isolate electrons. The electrolyte was 1 M bis(trifluoromethane) sulfonimide lithium salt (LiTFSI) with 1% LiNO₃ dissolved in a mixture of 1,3-dioxolane (DOL) and dimethoxyethane (DME) (1:1 by volume). The amount of electrolyte in the coin cell with the areal sulfur loading of 0.49 mg cm⁻² is 50 μ L. When the areal sulfur loading is increased to 3.51 and 4.4 mg cm⁻², the corresponding amount of electrolyte is 250 and 300 μ L, respectively. The discharge/charge measurements were conducted using a Neware battery test system (Neware Technology Co.). Before testing, the cells were aged for 24 h. Cyclic voltammetry (CV) and electrochemical impedance spectroscopy (EIS) measurements were performed on CHI660D electrochemical workstation. The scan rate for CV measurements was set as to be 0.1 mV s⁻¹, and the DC voltage was kept at open-circuit voltage and an AC voltage of 5 mV in amplitude was applied with a frequency of 200 kHz–20 mHz in EIS measurements.

Structure Characterization. X-ray diffraction patterns (XRD) were obtained with a D/MAX-2400 diffractometer using Cu $K\alpha$ radiation (40 kV, 100 mA, $\lambda = 1.54056$ Å). The nitrogen adsorption/desorption data were recorded at the liquid nitrogen temperature (77 K) using a Micromeritics ASAP 2020 M apparatus. The samples were degassed at 200 °C under vacuum for 3 h prior to the measurement. Pore size distribution (PSD) was derived from the adsorption branch of the isotherms using the Barrett–Joyner–Halenda (BJH) model. Total pore volumes were calculated from the amount adsorbed at a relative pressure (P/P_0) of 0.99. Scanning electron microscope (SEM) images were obtained with a JSM-6700F field-emission scan electron microscope. Thermo gravimetric analysis (TGA) was measured with a STA449 F3 Jupiter thermo gravimetric analyzer (NETZSCH), at a

heating rate of 10 °C min⁻¹ in nitrogen atmosphere. UV–vis absorption spectroscopy was used to characterize the polysulfide species and their contents in the electrolyte after the cells completed a certain number of cycles.

ASSOCIATED CONTENT

Supporting Information

The Supporting Information is available free of charge on the ACS Publications website at DOI: 10.1021/acsnano.6b08627.

TGA and XRD data, SEM images, typical photographs of the coating process, characterization of carbon, constitutional formula of dithiothreitol, Vitamin C, and glutathione, characteristics of various carbon–sulfur composites reported in literatures and additional related electrochemical data (PDF)

AUTHOR INFORMATION

Corresponding Authors

*E-mail: yang201079@126.com.

*E-mail: smhuang@wzu.edu.cn.

ORCID

Zhi Yang: 0000-0002-9265-5041

Notes

The authors declare no competing financial interest.

ACKNOWLEDGMENTS

The work was supported in part by grants from NSFC (51572197, 21273163, 21475096 and 51420105002).

REFERENCES

- (1) Ji, X. L.; Nazar, L. F. Advances in Li–S Batteries. *J. Mater. Chem.* **2010**, *20*, 9821–9826.
- (2) Bruce, P. G.; Freunberger, S. A.; Hardwick, L. J.; Tarascon, J. M. Li–O₂ and Li–S Batteries with High Energy Storage. *Nat. Mater.* **2012**, *11*, 19–29.
- (3) Yang, Y.; Zheng, G. Y.; Cui, Y. Nanostructured Sulfur Cathodes. *Chem. Soc. Rev.* **2013**, *42*, 3018–3032.
- (4) Yu, M. P.; Ma, J. S.; Song, H. Q.; Wang, A. J.; Tian, F. Y.; Wang, Y. S.; Qiu, H.; Wang, R. M. Atomic Layer Deposited TiO₂ on a Nitrogen-Doped Graphene/Sulfur Electrode for High Performance Lithium–Sulfur Batteries. *Energy Environ. Sci.* **2016**, *9*, 1495–1503.
- (5) Manthiram, A.; Fu, Y. Z.; Su, Y. S. Challenges and Prospects of Lithium–Sulfur Batteries. *Acc. Chem. Res.* **2013**, *46*, 1125–1134.
- (6) Pang, Q.; Kundu, D.; Cuisinier, M.; Nazar, L. F. Surface-Enhanced Redox Chemistry of Polysulfides on a Metallic and Polar Host for Lithium–Sulphur Batteries. *Nat. Commun.* **2014**, *5*, 4759.
- (7) Zhang, J. T.; Hu, H.; Zhen, L.; Lou, X. W. Double-Shelled Nanocages with Cobalt Hydroxide Inner Shell and Layered Double Hydroxides Outer Shell as High-Efficiency Polysulfide Mediator for Lithium–Sulfur Batteries. *Angew. Chem., Int. Ed.* **2016**, *55*, 3982–3986.
- (8) Zhang, Q. F.; Wang, Y. P.; Seh, Z. W.; Fu, Z. H.; Zhang, R. F.; Cui, Y. Understanding the Anchoring Effect of Two-Dimensional Layered Materials for Lithium–Sulfur Batteries. *Nano Lett.* **2015**, *15*, 3780–3786.
- (9) Zhao, M. Q.; Zhang, Q.; Huang, J. Q.; Tian, G. L.; Nie, J. Q.; Peng, H. J.; Wei, F. Unstacked Double-Layer Templated Graphene for High-Rate Lithium–Sulphur Batteries. *Nat. Commun.* **2014**, *5*, 3410.
- (10) Zhang, K.; Zhao, Q.; Tao, Z. L.; Chen, J. Composite of Sulfur Impregnated in Porous Hollow Carbon Spheres as the Cathode of Li–S Batteries with High Performance. *Nano Res.* **2013**, *6*, 38–46.
- (11) Sun, Q.; He, B.; Zhang, X. Q.; Lu, A. H. Engineering of Hollow Core-Shell Interlinked Carbon Spheres for Highly Stable Lithium–Sulfur Batteries. *ACS Nano* **2015**, *9*, 8504–8513.
- (12) Tao, X. Y.; Wang, J. G.; Ying, Z. G.; Cai, Q. X.; Zheng, Y.; Gan, Y.; Huang, H.; Xia, Y.; Liang, C.; Zhang, W.; Cui, Y. Strong Sulfur

Binding with Conducting Magnéli-Phase TinO_{2n-1} Nanomaterials for Improving Lithium–Sulfur Batteries. *Nano Lett.* **2014**, *14*, 5288–5294.

(13) Liang, X.; Hart, C.; Pang, Q.; Garsuch, A.; Weiss, T.; Nazar, L. F. A Highly Efficient Polysulfide Mediator for Lithium–Sulfur Batteries. *Nat. Commun.* **2015**, *6*, 5682.

(14) Li, Z.; Zhang, J. T.; Lou, X. W. Hollow Carbon Nanofibers Filled with MnO₂ Nanosheets as Efficient Sulfur Hosts for Lithium–Sulfur Batteries. *Angew. Chem., Int. Ed.* **2015**, *54*, 12886–12890.

(15) Su, Y. S.; Manthiram, A. Lithium–Sulphur Batteries with a Microporous Carbon Paper as a Bifunctional Interlayer. *Nat. Commun.* **2012**, *3*, 1166.

(16) Hwang, J. Y.; Kim, H. M.; Lee, S. K.; Lee, J. H.; Abouimrane, A.; Khaleel, M. A.; Belharouak, I.; Manthiram, A.; Sun, Y. K. High-Energy, High-Rate, Lithium–Sulfur Batteries: Synergetic Effect of Hollow TiO₂-Webbed Carbon Nanotubes and a Dual Functional Carbon-Paper Interlayer. *Adv. Energy Mater.* **2016**, *6*, 1501480.

(17) Wang, H. Q.; Zhang, W. C.; Liu, H. K.; Guo, Z. P. Strategy for Configuration of an Integrated Flexible Sulfur Cathode for High-Performance Lithium–Sulfur Batteries. *Angew. Chem., Int. Ed.* **2016**, *55*, 3992–3996.

(18) Huang, J. Q.; Zhuang, T. Z.; Zhang, Q.; Peng, H. J.; Chen, C. M.; Wei, F. Permselective Graphene Oxide Membrane for Highly Stable and Anti-Self-Discharge Lithium–Sulfur Batteries. *ACS Nano* **2015**, *9*, 3002–3011.

(19) Xiao, Z. B.; Yang, Z.; Wang, L.; Nie, H. G.; Zhong, M. E.; Lai, Q. Q.; Xu, X. J.; Zhang, L. J.; Huang, S. M. A Lightweight TiO₂/Graphene Interlayer, Applied as a Highly Effective Polysulfide Absorbent for Fast, Long-Life Lithium–Sulfur Batteries. *Adv. Mater.* **2015**, *27*, 2891–2898.

(20) Deng, Z. F.; Zhang, Z.; Lai, Y. Q.; Liu, J.; Lie, J.; Liu, Y. X. Electrochemical Impedance Spectroscopy Study of a Lithium/Sulfur Battery: Modeling and Analysis of Capacity Fading. *J. Electrochem. Soc.* **2013**, *160*, A553–A558.

(21) Hagen, M.; Feisthammel, G.; Fanz, P.; Grossmann, H. T.; Dorfler, S.; Tubke, J.; Hoffmann, M. J.; Borner, D.; Joos, M.; Althues, H. Sulfur Cathodes with Carbon Current Collector for Li–S Cells. *J. Electrochem. Soc.* **2013**, *160*, A996–A1002.

(22) Xin, S.; Gu, L.; Zhao, N. H.; Yin, Y. X.; Zhou, L. J.; Guo, Y. G.; Wan, L. J. Smaller Sulfur Molecules Promise Better Lithium–Sulfur Batteries. *J. Am. Chem. Soc.* **2012**, *134*, 18510–18513.

(23) Al Salem, H.; Babu, G.; Rao, C. V.; Arava, L. M. R. Electrocatalytic Polysulfide Traps for Controlling Redox Shuttle Process of Li–S Batteries. *J. Am. Chem. Soc.* **2015**, *137*, 11542–11545.

(24) Yuan, Z.; Peng, H. J.; Hou, T. Z.; Huang, J. Q.; Chen, C. M.; Wang, D. W.; Cheng, X. B.; Wei, F.; Zhang, Q. Powering Lithium–Sulfur Battery Performance by Propelling Polysulfide Redox at Sulfiphilic Hosts. *Nano Lett.* **2016**, *16*, 519–527.

(25) Mahdokht, S.; Abozar, A.; Phillip, S.; Christopher, D. E.; Parama, C. B.; Kristina, K.; Armaghan, F.; Marzieh, B.; Mustafa, M. M.; Adam, S. B.; Thomas, R.; Peter, J. M.; Matthew, R. H.; Anthony, F. H.; Mainak, M. Suppressed Polysulfide Crossover in Li–S Batteries through a High-Flux Graphene Oxide Membrane Supported on a Sulfur Cathode. *ACS Nano* **2016**, *10*, 7768–7779.

(26) Peng, H. J.; Zhang, Z. W.; Huang, J. Q.; Zhang, G.; Xie, J.; Xu, W. T.; Shi, J. L.; Chen, X.; Cheng, X. B.; Zhang, Q. A Cooperative Interface for Highly Efficient Lithium–Sulfur Batteries. *Adv. Mater.* **2016**, *28*, 9551–9558.

(27) Xu, N.; Qian, T.; Liu, X. J.; Liu, J.; Chen, Y.; Yan, C. L. Greatly Suppressed Shuttle Effect for Improved Lithium Sulfur Battery Performance through Short Chain Intermediates. *Nano Lett.* **2017**, *17*, 538–543.

(28) Zhao, H. Z.; Lu, Z. X.; Bie, X. M.; Lu, F. G.; Liu, Z. M. Lipase Catalyzed Acidolysis of Lard with Capric Acid in Organic Solvent. *J. Food Eng.* **2007**, *78*, 41–46.

(29) Cramer, C. N.; Haselmann, K. F.; Olsen, J. V.; Nielsen, P. K. Disulfide Linkage Characterization of Disulfide Bond-Containing Proteins and Peptides by Reducing Electrochemistry and Mass Spectrometry. *Anal. Chem.* **2016**, *88*, 1585–1592.

- (30) Lamoureux, G. V.; Whitesides, G. M. Synthesis of Dithiols as Reducing Agents for Disulfides in Neutral Aqueous Solution and Comparison of Reduction Potentials. *J. Org. Chem.* **1993**, *58*, 633–641.
- (31) Nordstrand, K.; Aslund, F.; Holmgren, A.; Otting, G.; Berndt, K. D. NMR Structure of *Escherichia Coli* Glutaredoxin 3-Glutathione Mixed Disulfide Complex: Implications for the Enzymatic Mechanism. *J. Mol. Biol.* **1999**, *286*, 541–552.
- (32) Xiao, Z. B.; Yang, Z.; Nie, H. G.; Lu, Y. Q.; Yang, K. Q.; Huang, S. M. Porous Carbon Nanotubes Etched by Water Steam for High-Rate Large-Capacity Lithium–Sulfur Batteries. *J. Mater. Chem. A* **2014**, *2*, 8683–8689.
- (33) Chung, S. H.; Manthiram, A. Carbonized Eggshell Membrane as a Natural Polysulfide Reservoir for Highly Reversible Li-S Batteries. *Adv. Mater.* **2014**, *26*, 1360–1365.
- (34) Song, M. K.; Zhang, Y. G.; Cairns, E. J. A Long-Life, High-Rate Lithium/Sulfur Cell: A Multifaceted Approach to Enhancing Cell Performance. *Nano Lett.* **2013**, *13*, 5891–5899.
- (35) Li, G. C.; Li, G. R.; Ye, X. P.; Gao, X. P. A Polyaniline-Coated Sulfur/Carbon Composite with an Enhanced High-Rate Capability as a Cathode Material for Lithium/Sulfur Batteries. *Adv. Energy Mater.* **2012**, *2*, 1238–1245.
- (36) Wang, L.; Yang, Z.; Nie, H. G.; Gu, C. C.; Hua, W. X.; Xu, X. J.; Chen, X. A.; Chen, Y.; Huang, S. M. A Lightweight Multifunctional Interlayer of Sulfur–Nitrogen Dual-Doped Graphene for Ultrafast, Long-life Lithium–Sulfur Batteries. *J. Mater. Chem. A* **2016**, *4*, 15343–15352.
- (37) Tao, X. Y.; Wang, J. G.; Liu, C.; Wang, H. T.; Yao, H. B.; Zheng, G. Y.; Seh, Z. W.; Cai, Q. X.; Li, W. Y.; Zhou, G. M.; Zu, C. X.; Cui, Y. Balancing Surface Adsorption and Diffusion of Lithium–Polysulfides on Nonconductive Oxides for Lithium–Sulfur Battery Design. *Nat. Commun.* **2016**, *7*, 11203.
- (38) Zhou, Y.; Zhou, C. G.; Li, Q. Y.; Yan, C. J.; Han, B.; Xia, K. S.; Gao, Q.; Wu, J. P. Enabling Prominent High-Rate and Cycle Performances in One Lithium–Sulfur Battery: Designing Permelective Gateways for Li⁺ Transportation in Holey-CNT/S Cathodes. *Adv. Mater.* **2015**, *27*, 3774–3781.
- (39) Hu, H.; Cheng, H. Y.; Liu, Z. F.; Li, G. J.; Zhu, Q. C.; Yu, Y. *In Situ* Polymerized PAN-Assisted S/C Nanosphere with Enhanced High-Power Performance as Cathode for Lithium/Sulfur Batteries. *Nano Lett.* **2015**, *15*, 5116–5123.
- (40) Lv, D. P.; Zheng, J. M.; Li, Q. Y.; Xie, X.; Ferrara, S.; Nie, Z. M.; Mehdi, L. B.; Browning, N. D.; Zhang, J. G.; Graff, G. L.; Liu, J.; Xiao, J. High Energy Density Lithium–Sulfur Batteries: Challenges of Thick Sulfur Cathodes. *Adv. Energy Mater.* **2015**, *5*, 1402290.
- (41) Li, Y. J.; Zhan, H.; Liu, S. Q.; Huang, K. L.; Zhou, Y. H. Electrochemical Properties of the Soluble Reduction Products in Rechargeable Li/S Battery. *J. Power Sources* **2010**, *195*, 2945–2949.
- (42) Barchasz, C.; Molton, F.; Duboc, C.; Lepretre, J. C.; Patoux, S.; Alloin, F. Lithium/Sulfur Cell Discharge Mechanism: An Original Approach for Intermediate Species Identification. *Anal. Chem.* **2012**, *84*, 3973–3980.